

EFFECTS OF A COMPANION STAR ON SLOW NOVA OUTBURSTS – TRANSITION FROM STATIC TO WIND EVOLUTIONS

MARIKO KATO

Department of Astronomy, Keio University, Hiyoshi 4-1-1, Kouhoku-ku, Yokohama 223-8521, Japan:

AND

IZUMI HACHISU

Department of Earth Science and Astronomy, College of Arts and Sciences, University of Tokyo, Komaba 3-8-1, Meguro-ku, Tokyo 153-8902, Japan;

to appear in *ApJ*, 2011

ABSTRACT

Two types of nova evolutions can be realized in low-mass white dwarfs of $\sim 0.5-0.7 M_{\odot}$, i.e., an evolution with optically thick winds like in usual classical novae, or an another type of evolution without them like in the symbiotic nova PU Vul. The latter type is characterized by spectra of no indication of strong winds as well as a long-lasting flat optical peak in its light curve. We propose a transition from no-optically thick wind evolution to usual evolution with optically thick winds as a new outburst model for slow novae that show a relatively long-lasting multipeak phase followed by a wind phase like in the slow novae V723 Cas, HR Del, and V5558 Sgr. We calculated nova envelopes with one-dimensional approximation of the companion's effects and found that when the companion star is deeply embedded in the extended nova envelope, the structure of static envelope approaches that of the optically thick wind solution. Thus, the transition from static to wind solution is triggered by the effect of the companion. The transition occurs in a close binary nova like V723 Cas, but is not triggered in a long period binary like PU Vul. We reconfirm our previous results that the frictional energy deposition is negligibly small in almost all of hydrogen/helium novae because of the low envelope density at the orbit.

Subject headings: binaries: close — novae, cataclysmic variables — stars: individual (V723 Cas, HR Del, V5558 Sgr) — stars: winds, outflows

1. INTRODUCTION

Nova is a thermonuclear runaway event on a mass-accreting white dwarf (WD). During a nova outburst, the envelope on the WD expands considerably and engulfs its mass-donating companion unless it is a wide binary. As the companion orbits in the nova envelope, frictional processes between the envelope and the companion produces thermal energy. In 1980's, it was believed that these frictional processes play an important role to eject the envelope and to shorten the nova duration by a factor of 10 or more (MacDonald et al. 1985; Livio et al. 1990; Shanker et al. 1991). This idea was originally proposed to reconcile observed short durations of classical novae (~ 1 yr) with long timescales of nuclear burning (~ 1000 yr). However, the drag energy deposition is not effective for mass ejection in the common envelope phase of novae because the envelope masses are too small to produce drag-energy enough to eject the envelope (Kato & Hachisu 1991a,b).

In the beginning of 1990's, opacity tables were revised (OPAL opacity: Iglesias & Rogers 1996), of which a prominent peak at $\log T(\text{K}) \sim 5.2$ is strong enough to accelerate optically thick winds even in relatively less massive WDs of $\sim 0.6 M_{\odot}$. This wind is as massive as $10^{-4} M_{\odot} \text{ yr}^{-1}$ or more. The nova duration is drastically reduced so that the theoretical duration becomes comparable to the observed one (e.g., Kato & Hachisu 1994; Prialnik & Kovetz 1995). Once the wind occurs, frictional effects are ineffective, because the density at the orbit is too low to produce large energy deposition. Moreover, the wind is accelerated deep inside the orbit and the wind velocity has already reached the escape velocity at the orbit. Thus, once the optically thick winds oc-

cur, the presence of a companion has virtually no effects on the envelope structure nor on the duration of nova outbursts (Kato & Hachisu 1994).

There are observational indications that frictional process is not effective in nova outbursts. If the frictional process is very effective in mass ejection, there should be a clear dependence of nova light curve shapes on the orbital period, but no such properties are known. For example, the recurrent nova RS Oph shows a very fast development of optical light curve (Hachisu et al. 2006) similar to that of U Sco. RS Oph is a long period binary of $P_{\text{orb}} = 456$ days (Fekel et al. 2000), so that the WD photosphere does not reach the companion even at the maximum expansion (Hachisu et al. 2006). Therefore, the frictional processes of companion do not work in the whole period of the nova outburst. On the other hand, U Sco is a short period binary of $P_{\text{orb}} = 1.23$ days (Schaefer & Ringwald 1995) and the companion star is engulfed deeply in the envelope during the outburst. The 1999 and 2010 outbursts of U Sco were densely observed, but there is no indication for additional acceleration nor enhanced mass ejection due to the companion motion (Hachisu et al. 2000).

We have analyzed a number of nova light curves with the universal decline law based on the optically thick winds (Hachisu & Kato 2006, 2007, 2010; Hachisu et al. 2006, 2008; Kato & Hachisu 1994, 2009; Kato et al. 2009). If the companion motion strongly contributes to the acceleration of matter, there should be a change in the decline rates of light curves when the companion reappears from the extended envelope of the WD. However, none of them show a particular change in the light curves before and after the epoch that the companion reappeared from the envelope. We refer two examples of classical novae, with a densely observed light

curve and known orbital period: V1500 Cyg ($P_{\text{orb}} = 0.14$ days, see the light curves in Figure 13 of Hachisu & Kato 2006); the companion emerged on days ~ 50 but nothing had happened, and also V458 Vul ($P_{\text{orb}} = 0.59$ days, in Figure 26 of Hachisu & Kato 2010); the companion emerged on days ~ 60 but nothing happened. These are good counterevidence against the effectiveness of frictional process. Therefore, we emphasize that frictional processes are not effective in novae whenever strong optically thick winds blow.

In our theoretical models, optically thick winds always occur in nova outbursts on massive WDs ($\gtrsim 0.7 M_{\odot}$) but do not occur in less massive WDs ($\lesssim 0.5 M_{\odot}$). Between them, i.e., $\sim 0.5\text{--}0.7 M_{\odot}$, both types of nova evolutions, with/without optically thick winds, are realized for the same WD mass (Kato & Hachisu 2009). When no optically thick winds are accelerated, nova outbursts show a slow evolution with a long-lasting flat optical maximum, in contrast with usual classical novae that show a sharp optical maximum caused by a rapid evolution due to wind mass loss (Kato 2011). The first example of such no-optically thick wind evolution is the symbiotic nova PU Vul, in which a flat optical peak lasted 3000 days and showed very quiet spectra indicating no strong winds (Kato et al. 2011).

Kato & Hachisu (2009) presented an idea that a nova outburst started in a state of no-optically thick winds (we call this “static evolution”) and then possibly changes to be in a state of optically thick winds (“wind evolution”). They also suggested that such a transition may accompany violent activities such as oscillatory behaviors in the light curves of some slow novae.

Here, we present an idea that a companion star plays a role in changing the nova envelope structure from “static” to “wind.” If this occurs in low-mass WDs, it may relate to the peculiar light curves of slow novae. As an application of such a transition to slow novae like V723 Cas, we have examined effects of a companion star with one-dimensional (1D) approximation of nova envelopes. In Section 2, we briefly introduce our method. Numerical results are presented in Section 3. Applications to slow novae appear in Section 4. Discussion and summary follow in Sections 5 and 6.

2. ENVELOPE MODEL

We consider low-mass WDs in which no optically thick winds are accelerated in the beginning of nova outbursts. This may happen in low-mass WDs ($\lesssim 0.7 M_{\odot}$) under some conditions of the initial envelope mass and chemical composition (see Kato & Hachisu 2009, for more details). After a thermonuclear runaway sets in, the envelope greatly expands and the optical brightness increases to reach a flat maximum. We approximate the nova evolution by a sequence of hydrostatic solutions when no optically thick winds occur, and by a sequence of steady-state solutions with optically thick winds when it occurs. In these sequences of solutions the envelope mass is decreasing due to nuclear burning and wind mass loss if it occurs, from which we calculate evolution timescale. This quasi-evolution is a good approximation because the thermal/dynamical timescale between two successive solutions are short enough compared with the evolution timescale of novae.

For static solutions we solve the equations of hydrostatic balance, mass continuity, radiative diffusion, and conservation of energy, from the bottom of the hydrogen-rich envelope through the photosphere assuming spherical symmetry. For wind solutions, we solve the equation of motion assuming

steady-state, instead of hydrostatic balance (Kato & Hachisu 1994). Convective energy transport is calculated in static solutions using the mixing length theory with the ratio of mixing length to pressure scale height $\alpha = 1.5$ (see Kato & Hachisu 2009, for effects of the α parameter on static solutions). The occurrence of optically thick winds is detected by the condition described in Kato (1985). In our numerical calculations, we adopt more than 8000 meshes and always insert ~ 1700 meshes in the interacting region between $r = R_{\text{orb}} - R_a$ and $r = R_{\text{orb}} + R_a$, where R_{orb} is the position of the companion from the WD center and R_a is the accretion radius as defined below. The chemical composition of the envelope is simply assumed to be uniform with the composition of $X = 0.55$, $Y = 0.23$, $CNO = 0.2$, and $Z = 0.02$, which are representative values for slow novae (see Table 1 of Hachisu & Kato 2006). We assume an $0.55 M_{\odot}$ WD and an $0.4 M_{\odot}$ main-sequence (MS) companion that fills its Roche lobe unless otherwise stated. This $0.4 M_{\odot}$ is close to an upper limit of the companion mass, $0.44 M_{\odot}$, in a binary system with thermally stable mass transfer ($q = M_{\text{comp}}/M_{\text{WD}} \lesssim 0.8$). We assume such a large mass because a more massive companion has larger effects on the WD envelope.

Three effects of the companion on the WD envelope are considered here: (1) spun-up by the companion motion, (2) gravity of the companion star, and (3) drag luminosity due to frictional energy deposition. We incorporated these effects in our computer code as explained in the following subsections.

2.1. Centrifugal Force

In the very beginning of a nova outburst, the envelope has so small specific angular momentum compared with the specific orbital angular momentum. After the envelope expands to a giant size, it begins to counterrotate on the rotating frame with the companion due to conservation of the local angular momentum. The outer part of the envelope may be spun up due to frictional effects of the companion motion. We incorporate the effect of centrifugal force in our 1D code. We modified the equation of hydrostatic balance as

$$\frac{1}{\rho} \frac{dP}{dr} = -\frac{GM_r}{r^2} + r\omega^2, \quad (1)$$

where ω is the angular velocity. This is a 1D approximation that may represent envelope structure in the equatorial plane. Here we introduce the effective mass parameter f and rewrite Equation (1) as

$$\frac{1}{\rho} \frac{dP}{dr} = -\frac{GM_r}{r^2} f, \quad (2)$$

$$f \equiv 1 - \frac{\omega^2 r^3}{GM_r}. \quad (3)$$

The factor f represents the degree how much the gravity is effectively reduced due to the centrifugal force. In other words, the effective mass decreases to fM_r . We, hereafter, call f the mass reducing factor.

We assumed a simplified rotation law for the envelope; a rigid rotation in the inner part of the envelope ($r < R_{\Omega}$) and a Keplerian-like rotation in the outer part ($r \geq R_{\Omega}$). Since the envelope is spun up by the companion motion inside the outer Lagrange point, we define the rigid rotation radius as $R_{\Omega} = R_{\text{orb}} + 1.2 \times R_{\text{comp}}$ because the outer Lagrange point is located at $\sim 1.2 \times R_{\text{comp}}$ from the companion center.

For the inner part ($r < R_{\Omega}$), we assume a solid rotation with an angular velocity of $\omega_0 = \eta V_{\text{orb}}/R_{\text{orb}}$, here η is a parameter

that represents the ratio of the angular velocity of the envelope to that of the companion, $\Omega = V_{\text{orb}}/R_{\text{orb}}$. In other words, η means the ratio of the envelope velocity to the companion velocity at the orbit.

For the outer part ($r \geq R_{\Omega}$) we assume that the rotation velocity of the envelope varies as $r^{-1/2}$ as the Keplerian velocity does. In this case, the angular velocity ω changes as $r^{-3/2}$, and can be expressed as $\omega = \eta V_{\text{orb}} R_{\text{orb}}^{-1} R_{\Omega}^{3/2} r^{-3/2}$. Using Kepler's law $V_{\text{orb}}^2 = G(M_{\text{WD}} + M_{\text{comp}})/R_{\text{orb}}$, the specific centrifugal force can be rewritten as

$$r\omega^2 = \eta^2 \left(\frac{R_{\Omega}}{R_{\text{orb}}}\right)^3 \frac{G(M_{\text{WD}} + M_{\text{comp}})}{r^2}. \quad (4)$$

Then f becomes

$$f = 1 - \eta^2 \left(\frac{R_{\Omega}}{R_{\text{orb}}}\right)^3, \quad \text{for } r \geq R_{\Omega}. \quad (5)$$

Here we use $M_r = M_{\text{WD}} + M_{\text{comp}}$ at $r \geq R_{\Omega}$. Thus, f is constant at $r \geq R_{\Omega}$. Approximations of these centrifugal force and 1D approximation are discussed in Sections 5.2 and 5.3.

2.2. Gravity of the Secondary

In our 1D approximation, we have simply assumed that the companion is distributed uniformly within a shell of $r = R_{\text{orb}} \pm R_{\text{comp}}$. Since the envelope mass (10^{-3} to $10^{-6} M_{\odot}$) is much smaller than that of the companion ($M_{\text{comp}} = 0.4 M_{\odot}$), the change of M_r is essentially due to the mass distribution of the companion, i.e., $M_r = M_{\text{WD}}$ inside the radius of $r = R_{\text{orb}} - R_{\text{comp}}$, and $M_r = M_{\text{WD}} + M_{\text{comp}}$ outside the radius of $r = R_{\text{orb}} + R_{\text{comp}}$. These treatments are essentially the same as those in Kato & Hachisu (1994).

Figure 1 shows examples of the angular velocity ω , mass distribution M_r , mass reducing factor f , and effective mass fM_r for our envelope models. Here, f is unity in the deep inside the envelope ($r \ll R_{\text{orb}}$), but 0.971, 0.741, 0.578 and 0.418 in the outer region ($r \geq R_{\Omega}$) for $\eta = 0.1, 0.3, 0.383,$ and 0.45 , respectively. When $\eta = 0.383$ ($f = 0.578$), we have $(0.55 M_{\odot} + 0.4 M_{\odot}) \times 0.578 = 0.55 M_{\odot}$ at $r \geq R_{\Omega}$, i.e., the companion gravity is almost canceled by the centrifugal force. A small peak of the effective mass appears near $\log r$ (cm) ~ 11.0 because M_r is constant (i.e., $M_{\text{WD}} + M_{\text{comp}}$) outside $r = R_{\text{orb}} + R_{\text{comp}}$, whereas ω begins to decrease from a bit outside, at $R_{\Omega} = R_{\text{orb}} + 1.2 \times R_{\text{comp}}$

2.3. Drag Luminosity

We treat the drag luminosity in spherical (1D) approximation in the same way as in the other previous works (Taam & Bodenheimer 1989; Livio et al. 1990; Kato & Hachisu 1991a,b, 1994). The drag luminosity generated in the region from r to $r + \delta r$ can be approximated as

$$\delta L_{\text{drag}} = \rho (V_{\text{orb}} - v_e)^3 \delta S, \quad (6)$$

where ρ is the density of the envelope, $V_{\text{orb}} - v_e$ is the relative velocity between the envelope and the companion star, δS is the cross-sectional area between a circular strip from r to $r + \delta r$ and a circle with the radius R_a , the center of which is located at the orbit, $r = R_{\text{orb}}$. Here the modified accretion radius, R_a , is defined as

$$R_a = \frac{R_0}{1 + (R_0/2H)^2}, \quad (7)$$

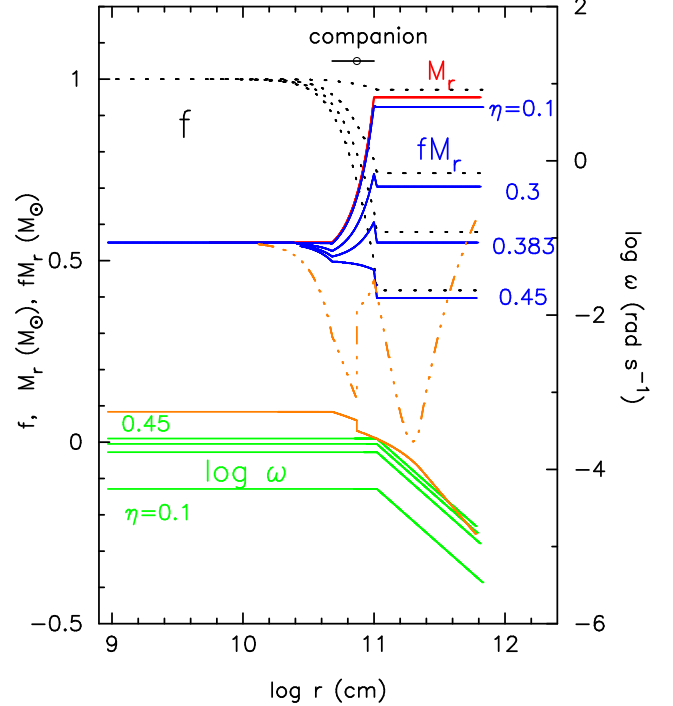


FIG. 1.— Adopted rotation law $\log \omega$ (green solid lines), gravity reducing factor f (black dotted lines), mass distribution M_r (red solid line), and effective mass, fM_r (blue solid lines), for a binary consisting of an $0.55 M_{\odot}$ WD and an $0.4 M_{\odot}$ MS companion with $\eta = 0.1, 0.3, 0.383,$ and 0.45 , from upper to lower for f and fM_r , but from lower to upper for $\log \omega$. The corresponding envelope structures are shown in Figure 4. The left/right edge of each line corresponds to the bottom/photosphere of the envelope. The location of the companion ($\log r$ (cm) = 10.869) and its size are indicated by a small open circle with a short horizontal bar. The orange solid and dash-three-dotted lines denote a trial rotation law and the corresponding effective mass, respectively (see Section 5.3).

where H is the local density scale height, and R_0 is the generalized Bondi (1952) radius defined by

$$R_0 = \frac{2GM_{\text{comp}}}{[(V_{\text{orb}} - v_e)^2 + C_s^2]}, \quad (8)$$

here C_s is the sound speed. In our 1D calculation the drag luminosity, δL_{drag} , is re-distributed over the entire spherical shell between r and $r + \delta r$. The total drag luminosity is

$$L_{\text{drag}} = \int \rho (V_{\text{orb}} - v_e)^3 \delta S, \quad (9)$$

where the integral region is from $R_{\text{orb}} - R_a$ to $R_{\text{orb}} + R_a$. We take the companion radius itself, R_{comp} , as the accretion radius instead of R_a when R_a is smaller than the companion radius. If both the density and R_a are constant in space, the drag luminosity becomes the standard expression, i.e.,

$$L_{\text{drag}} = \pi R_a^2 \rho (V_{\text{orb}} - v_e)^3 \quad (10)$$

(Taam & Bodenheimer 1989; Livio et al. 1990).

3. NOVA ENVELOPES WITH A COMPANION STAR

3.1. Structure of Static Envelopes

Figure 2 shows distribution of the temperature, density, diffusive luminosity, and the local Eddington luminosity. We do not include the effects of a companion for blue and green lines. The local Eddington luminosity (dotted lines) is defined as

$$L_{\text{Edd}} = \frac{4\pi c G M_r}{\kappa}, \quad (11)$$

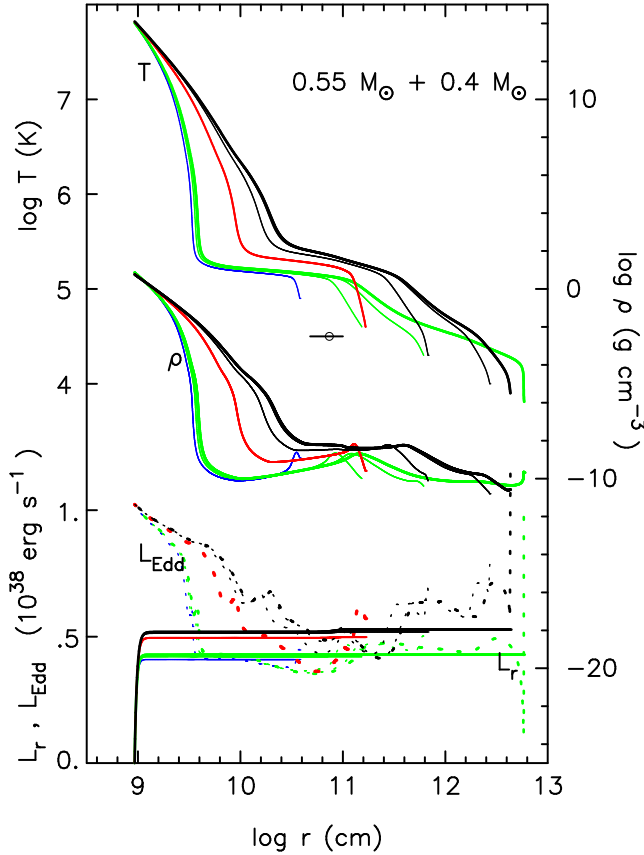


FIG. 2.— Distributions of the temperature T , density ρ , diffusive luminosity L_r , and the Eddington luminosity L_{Edd} defined by Equation (11). Each line corresponds to the envelope with the photospheric temperature of $\log T_{\text{ph}}(\text{K}) = 3.9$ (thick black lines), 4.0 (middle thin black lines), 4.3 (left thin black lines), and 4.6 (red lines). The location of the companion and its size are indicated by the small open circle with a short horizontal bar. For comparison, four solutions without the companion effects are added: $\log T_{\text{ph}}(\text{K}) = 3.81$ (green thick lines: right) and 4.3, 4.6 (green thin lines: right and left, respectively), and 4.9 (blue thin lines). The two envelopes of mass of $4.1 \times 10^{-5} M_{\odot}$.

where κ is the opacity. We used the OPAL opacity (Iglesias & Rogers 1996). As the opacity is a function of the temperature and density, and M_r is also the function of the radius (see Figure 1), the Eddington luminosity is also a local variable.

The blue and three green lines in Figure 2 depict the envelope solutions of $\log T_{\text{ph}}(\text{K}) = 4.9, 4.6, 4.3$ and 3.81 for the case of no companion star. These envelopes have essentially the same structure except for the surface region. As reported by Kato & Hachisu (2009), a static envelope has a core-halo structure of the density in which a large density inversion layer develops deep inside the photosphere. The density-inversion region corresponds to the super-Eddington region. The local Eddington luminosity has the deepest local minimum between $\log r(\text{cm}) \sim 10.0$ and 11.0, corresponding to the peak of the OPAL opacity at $\log T(\text{K}) \sim 5.2$. This density-inversion arises in order to keep hydrostatic balance in the super-Eddington region ($L_r > L_{\text{Edd}}$) as expected from the equation of hydrostatic balance (Kato & Hachisu 2009). Inefficient convections occur in the region of $L_r > L_{\text{Edd}}$ but are unable to carry all of the diffusive energy flux.

Black and red lines in Figure 2 indicate the models in which the companion's gravity and drag luminosity are incorporated. The three envelopes denoted by the black lines have very simi-

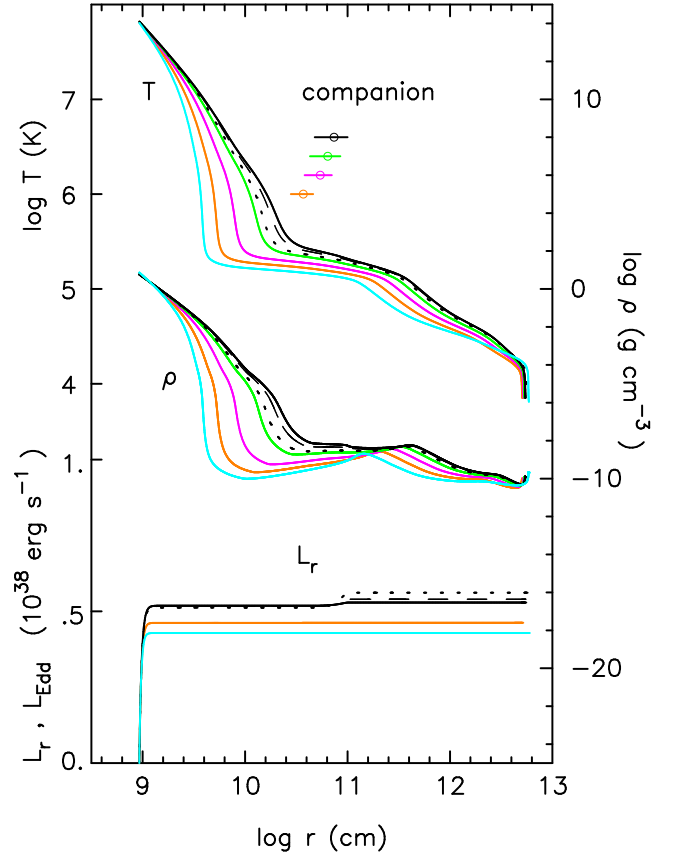


FIG. 3.— Same as Figure 2 but for static solutions with different companion masses. The photospheric temperature is $\log T_{\text{ph}}(\text{K}) = 3.85$ for all the solutions. $M_{\text{comp}} = 0.0$ (blue), 0.1 (brown), 0.2 (pink), 0.3 (green), and $0.4 M_{\odot}$ (black solid). Diffusive luminosity for $M_{\text{comp}} = 0.2$ and $0.3 M_{\odot}$ models are omitted to simplify the figure. The location of the companion are indicated by the small open circles with a short horizontal bar for $M_{\text{comp}} = 0.1, 0.2, 0.3$, and $0.4 M_{\odot}$ from left to right. Dashed and dotted lines indicate static solutions with enhanced drag luminosity by a factor of 2.8 and 10, respectively (see Section 5.2 for details).

lar structures at $\log r(\text{cm}) < 11.5$. The drag energy deposition is small as explained below. Therefore, the diffusive luminosity barely increases around the orbit in the model of $\log T_{\text{ph}}(\text{K}) = 3.9$, in which the drag luminosity deposition is 1.8% of the total flux.

Comparing these envelope models (black lines) with those without the companion effects (green and blue lines), we see that the envelope matter is significantly re-distributed due to the companion's effects. In the presence of the companion, the Eddington luminosity, outside the orbit is $L_{\text{Edd}} = 4\pi cG(M_{\text{WD}} + M_{\text{comp}})/\kappa$, which is larger than that without companion $L_{\text{Edd}} = 4\pi cGM_{\text{WD}}/\kappa$. This difference causes different energy flux as shown in Figure 2, $5.3 \times 10^{37} \text{ erg s}^{-1}$ in the model of black thick lines, whereas $4.3 \times 10^{37} \text{ erg s}^{-1}$ in the green thick lines. Therefore, these two envelopes are in different hydrostatic balance. A lower luminosity leads to a larger local super-Eddington region which causes a wider density-inversion region. The solution depicted by red lines has a photosphere just outside the companion orbit. Its photospheric luminosity is close to those of the solutions with the companion, but the structure is something between the two solutions with/without the companion.

Figure 3 compares structures of envelope models for $M_{\text{WD}} = 0.55 M_{\odot}$ among companion masses of $M_{\text{comp}} = 0.0, 0.1, 0.2, 0.3$, and $0.4 M_{\odot}$. For a larger companion mass, the density

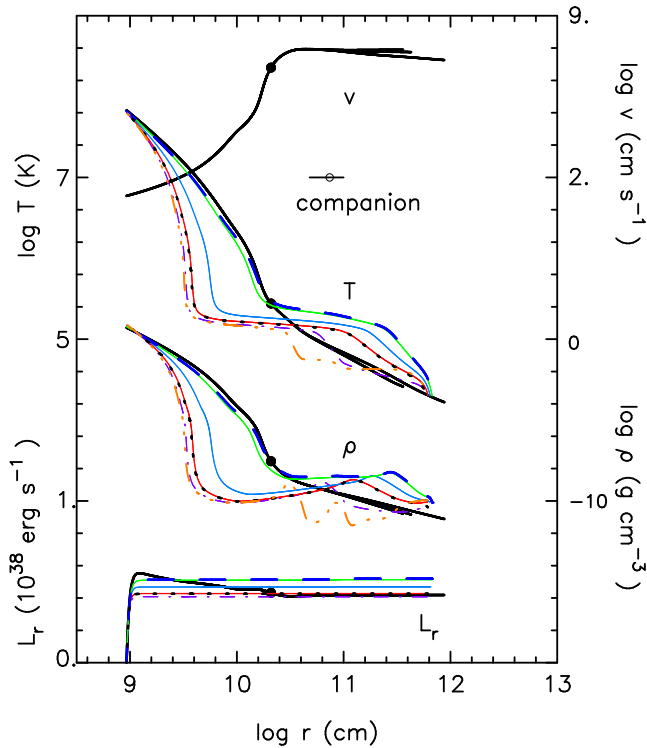


FIG. 4.— Comparison of the static and optically thick wind solutions with different rotation effect for the envelopes on a $0.55 M_{\odot}$ WD with a $0.4 M_{\odot}$ MS companion. Static solutions are depicted by colored lines, from upper to lower, $\eta=0$ (blue dashed line), 0.1 (green solid line), 0.3 (blue solid line), 0.383 (red solid line), and 0.45 (purple dash-dotted line). Dotted black lines denote a static solution without the companion effects, which is almost overlapped with the static solution of $f=0.383$ (red solid line). All the static solutions have a photospheric temperature of $\log T_{\text{ph}}$ (K) = 4.3. Optically thick wind solutions are depicted by the black solid line with a black dot that indicates the critical point at $R_{\text{cr}}=0.3 R_{\odot}$. Three solutions of $\eta=0.3, 0.383$, and 0.45 (the lower line in v , but the upper lines in T and ρ) are almost overlapped with each other as well as overlapped with the static solution of $\eta=0$ (blue dashed line) inside the critical point. The orange dash-three-dotted lines denote a test solution with different rotation law (same as orange lines in Figure 1) which will be discussed in Section 5.3.

inversion layer is smaller. In this way, the companion gravity has a role of redistribution of the envelope matter through different hydrostatic balance of gravity and pressure-gradient; a large luminosity causes larger radiation pressure gradient so that the matter is pushed outward. Dotted and dashed lines indicate the models with enhanced drag luminosities which will be explained in Section 5.2.

When the envelope rotates, the centrifugal force has an effect to reduce the gravity by the factor f . Figure 4 shows the envelope structure for $\log T_{\text{ph}}$ (K) = 4.3 with different angular velocity of $\eta=0.0, 0.1, 0.3, 0.383$, and 0.45. For a larger η , the centrifugal force becomes larger, which reduces the effective gravity. When $\eta=0.383$, the gravity of the companion ($M_{\text{comp}}=0.4 M_{\odot}$) is almost canceled as discussed earlier (see Figure 1), and the envelope has a structure very close to that of the solution without the companion effects. If we further increase η to 0.45, the envelope structure does not change much anymore except for the outer region where the temperature and density quickly drops (see the purple dash-dotted lines).

3.2. Structure of Wind Solutions

Figure 4 also shows the structures of optically thick wind solutions. The optically thick winds are accelerated due to the peak of OPAL opacity which locates deep inside the pho-

sphere. The wind velocity quickly increases around the critical point and reaches the terminal velocity deep inside the photosphere (Kato & Hachisu 1994).

Optically thick wind solutions hardly change its structure once it is accelerated even if there are some changes of acceleration source like opacity in the outside of the critical point. Figure 4 shows optically thick wind solutions for three different η , which correspond to different effective gravities as in Figure 1. As the critical point locates far inside the companion orbit and the winds are already accelerated there, the companion's gravity hardly changes the internal structure.

3.3. Drag Energy Deposition during Nova Outbursts

We already found that the drag energy deposition is small compared with the total luminosity. For example, it is only 3.2% of the photospheric luminosity in the model of $\log T_{\text{ph}}$ (K) = 3.85 (black solid line in Figure 3). This small contribution comes from the low density near the companion orbit because the drag luminosity is proportional to the density. Using Equation (10), we estimate it as

$$\begin{aligned} L_{\text{drag}} &\sim \pi R_{\text{a}}^2 \rho_{\text{orb}} V_{\text{orb}}^3 \\ &= \pi \times (3.3 \times 10^{10} \text{ cm})^2 \times 6.5 \times 10^{-9} \text{ g cm}^{-3} \times (410 \text{ km s}^{-1})^3 \\ &= 1.6 \times 10^{36} \text{ erg s}^{-1} \\ &= 0.030 L_{\text{ph}}, \end{aligned} \quad (12)$$

almost the same as our model value of 3.2%.

This low density is caused by the opacity peak as shown in Figure 2. The density is almost constant around the companion orbit. Thus, the drag luminosity is almost independent of the orbital size. If we assume a less massive companion, then we have a smaller R_{a} . For a smaller companion mass, on the other hand, the companion's Roche radius is smaller, so the companion comes into closer to the WD and the envelope's density is higher at the companion's orbit. However, a smaller radius (accretion radius) effect overcomes the effect of slightly higher density. As a result, a $0.1 M_{\odot}$ companion produces a hundred times smaller drag luminosity than an $0.4 M_{\odot}$ companion does. Thus, an $0.4 M_{\odot}$ companion gives almost an upper limit of the drag energy deposition for the $0.55 M_{\odot}$ WD model. During a nova outburst, the photospheric radius decreases with time and the density around the orbit slightly decreases with time as shown in Figure 2 in the case of static envelopes. Therefore, the drag luminosity decreases with time. In the case of rotating static envelopes, the density around the orbit is as small as or smaller than that for the non-rotating envelope as shown in Figure 4, so the drag luminosity is also too small.

In the case of optically thick wind envelopes, the density around the orbit is also as small as or much smaller than those of the static envelopes as shown in Figure 4. During the outburst, the density around the orbit decreases with time as will be shown later in Figure 7. In this way, we do not expect large drag luminosities during nova outbursts either in the static or in the wind evolution.

Figure 5 shows the ratio of the drag luminosity to the photospheric luminosity estimated for individual nova outbursts. A nova outburst starts from the uppermost point of each line, which corresponds to the peak luminosity, and moves downward as the envelope mass decreases with time. The drag luminosity quickly decreases with time because the density around the orbit quickly decreases in wind solutions (see Figure 7). The black lines depict three cases of classical novae. V838 Her is one of the fastest classical novae, which oc-

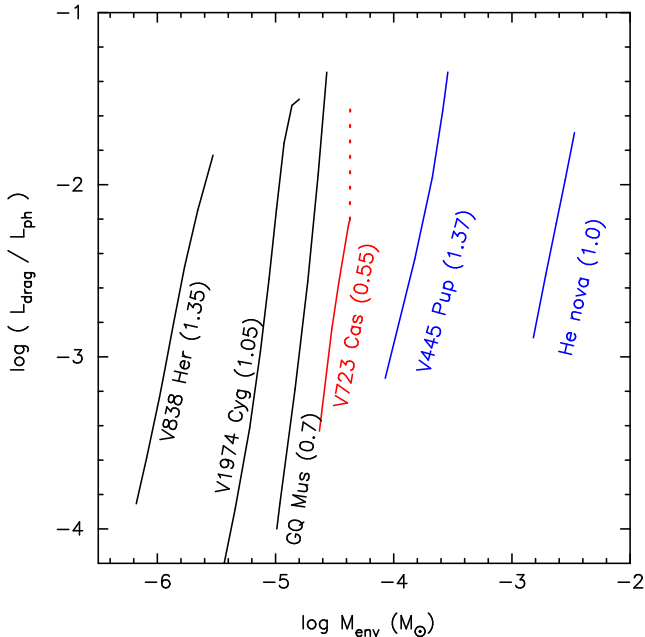


FIG. 5.— Ratio of the drag luminosity to the photospheric luminosity during nova outbursts. The top of each curve corresponds to the optical peak. The ratio decreases with time. The bottom point corresponds to the stage that the companion emerges from the WD photosphere. The WD mass of each outburst model is indicated after the object name in solar mass units. Three black lines depict classical novae with optically thick winds: V838 Her ($1.35 M_{\odot}$), V1974 Cyg ($1.05 M_{\odot}$), and GQ Mus ($0.7 M_{\odot}$). A red line is the composite model for V723 Cas ($0.55 M_{\odot}$), consisting of a static phase (top dotted part) and a wind phase (bottom solid part). The dotted part of V723 Cas represents the transition from the static to wind phase. Blue lines depict helium novae: V445 Pup ($1.37 M_{\odot}$) and a model for a $1.0 M_{\odot}$ WD. See text for more details.

curred on a very massive WD, thus the envelope mass is very small. Here we adopt the envelope structure taken from the light curve model of a $1.35 M_{\odot}$ WD calculated by Kato et al. (2009, model 2 in their Table 3) and a temporarily adopted $0.45 M_{\odot}$ companion at the separation of $a = 1.4 R_{\odot}$. The lowest point of the line corresponds to the stage at which the companion emerges from the photosphere and the companion effects vanish after that. In the same way, we have estimated the drag luminosities for the moderately fast nova V1974 Cyg (a $1.05 M_{\odot}$ WD model taken from Hachisu & Kato 2006) with an $0.2 M_{\odot}$ companion at $a = 0.85 R_{\odot}$, and for one of the slowest classical novae GQ Mus (an $0.7 M_{\odot}$ WD model taken from Hachisu et al. 2008) with an $0.1 M_{\odot}$ MS companion at $a = 0.6 R_{\odot}$. Here we adopt these parameters of the secondary, assuming they are in zero-age main sequence, which may not be accurate for each object. It is, however, enough for our purpose in estimating the drag luminosity, because it is not much affected by the choice of the secondary.

V838 Her and GQ Mus are the fastest and slowest classical novae, respectively. Thus, many other classical novae may fall in between these two lines like V1974 Cyg. We realize that the drag energy deposition is quite small. Even in the very early phase of the outburst, the ratio reaches only a few to several percent. Therefore, we reconfirm that the drag energy deposition does not contribute to the luminosity in classical novae.

Figure 5 also shows the case of a “transition nova,” which is a model for V723 Cas (see the next section for more details). The binary consists of an $0.55 M_{\odot}$ WD and an $0.4 M_{\odot}$ MS companion. The contribution of drag luminosity is also very small throughout the outburst.

The blue lines depict the case of helium nova outbursts. V445 Pup is only the known helium nova for which we adopt a $1.37 M_{\odot}$ WD model from Kato et al. (2008). The companion is assumed to be a $1.0 M_{\odot}$ helium star and $a = 2.3 R_{\odot}$. For comparison, we also added another case of helium nova of a $1.0 M_{\odot}$ WD (model taken from Kato et al. 2008), which has no observational counterpart but it is a theoretical purpose. For the companion, we assume an $0.8 M_{\odot}$ helium star, and $a = 2 R_{\odot}$. As shown in Figure 5 the drag luminosity is still very small.

4. APPLICATION TO SLOW NOVAE

4.1. Transition from Static to Wind Evolutions

Kato & Hachisu (2009) pointed out that two different types of nova evolutions, i.e., one is the evolution with optically thick winds and the other is without, can be realized in slow novae of a certain range of WD masses, $\sim 0.5 - 0.7 M_{\odot}$. For example, evolution of GQ Mus is explained by the sequence of optically thick wind solutions on a $\sim 0.7 M_{\odot}$ WD (Hachisu et al. 2008) while the evolution of PU Vul is described by a sequence of hydrostatic solutions on a $\sim 0.6 M_{\odot}$ WD (Kato et al. 2011).

A remarkable difference between these two evolutions appears in the optical light curve (Kato 2011). The wind-type novae have a sharp peak in the optical light curve, because massive optically thick wind carries away a large part of the envelope mass and the nova light curves decay quickly. On the other hand, no-optically thick wind novae have a long-lasting flat optical peak before the magnitude slowly decays, because the nova evolves very slowly and it stays at an extended low-temperature stage for a long time, which makes a long-lasting flat optical peak.

Kato & Hachisu (2009) presented an idea that a transition from the static evolution to the wind evolution could occur during an outburst. In such a case, the nova shows a flat optical peak with no indication of strong mass loss in the early phase of the outburst, followed by the decay like in normal novae with strong winds. Kato & Hachisu (2009) further suggested that such a transition accompanies some activities like oscillatory behavior in brightness, because the internal structures of static/wind solutions are very different and the relaxation process may cause some oscillatory features.

Such a transition, however, may need some triggering mechanism. PU Vul has a flat optical peak that lasted for 8 yr. This indicates that the static evolution is stable in a timescale of ~ 10 yr. We suppose that a transition to a wind evolution was not triggered in PU Vul because the structures of the static envelope are very different from those of the wind solutions. The static solution, however, changes its structure when a companion star disturbs the structure of a static envelope as shown in Section 3. This encourages us to further investigate our idea that the transition from the static to wind solution occurred in some slow novae.

4.2. Comparison of V723 Cas, HR Del, and V5558 Sgr with PU Vul

Figure 6 shows the observational light curve of PU Vul, V723 Cas, HR Del, and V5558 Sgr. PU Vul showed a flat optical maximum that lasted for 8 yr, neglecting the deep eclipse at $t = 2.2$ yr. The light curves of V723 Cas, HR Del, and V5558 Sgr are very similar to each other as already pointed out by many authors (Friedjung et al. 1992; Friedjung & Iijima 2002; Evans et al. 2003; Munari et al.

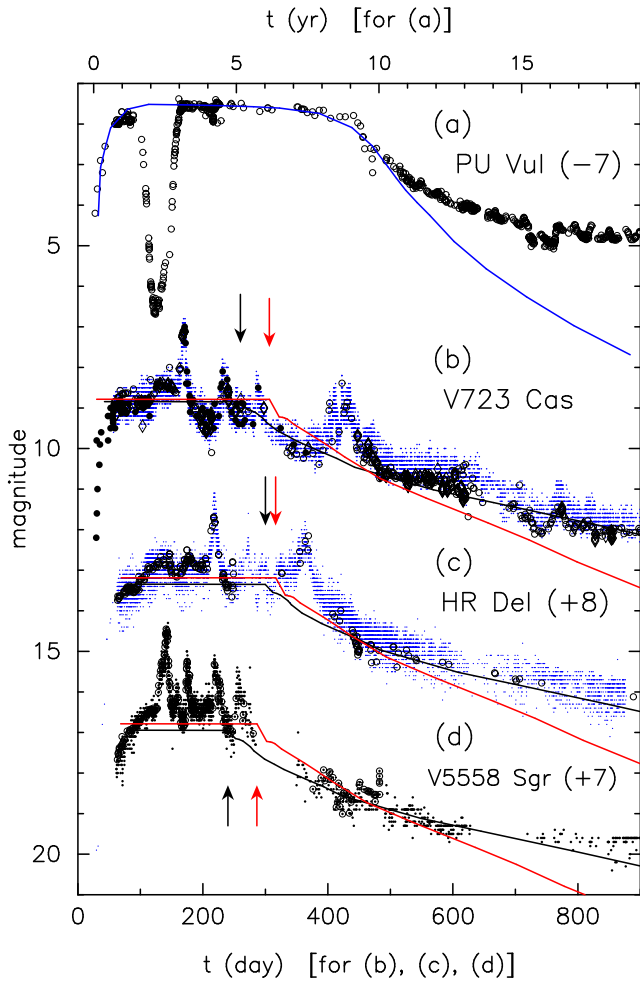


FIG. 6.— Comparison of light curves among PU Vul, V723 Cas, HR Del, and V5558 Sgr. PU Vul is shifted upward by 7 mag and HR Del and V5558 Cyg downward by 8 and 7 mag, respectively. The upper timescale is for PU Vul and lower one is for the other three novae. (a) PU Vul: data taken from Kato et al. (2011). The dips at $t = 2.2$ yr and 15.7 yr are eclipses. (b) V723 Cas: diamonds (Chochol & Pribulla 1997), filled small circles (IAUC Nos. 6213, 6214, 6227, 6233, 6256, 6283, 6331, 6358, 6428), open circles (AAVSO, V-mag), dots (AAVSO, visual). (c) HR Del: open circles (Stokes 1967; Pohl 1967; Nha 1967; Onderlička & Vetešník 1968; O’Connell 1968; Grygar 1969; Mollerus 1969; Mannery 1970; Barnes & Evans 1970, V), dots (AAVSO, visual). (d) V5558 Sgr: open circles (AAVSO, V), dots (AAVSO, visual). The solid lines indicate the composite light curve model of $0.55 M_{\odot}$ WD with $X = 0.55$, $C + O = 0.2$, $Z = 0.02$ (red line), and $0.6 M_{\odot}$ WD with the solar composition (black line). The arrows indicate the switching point from a static to a wind evolution: $\log T$ (K)=3.88 (red) and 3.93 (black).

2007). These novae have multiple peaks, showing an oscillatory variation around a certain magnitude. After that the magnitudes declined rather smoothly.

Resemblances in spectral evolutions were also suggested. V723 Cas shows very narrow emission/absorption lines in the spectra at the pre-maximum flat peak. The spectrum gradually changes to a pure absorption F-type supergiant before the optical maximum (Iijima et al. 1998). Note that PU Vul also shows F-type supergiant spectra with pure narrow absorptions, which are interpreted as static evolution (Kato et al. 2011). After the optical maximum, V723 Cas changes its spectrum to that of usual novae (Iijima et al. 1998) with many emission lines, some of which show a P Cygni profile (Iijima 2006; Evans et al. 2003). After that it entered the nebular phase (645–677 days after the discovery).

The spectral evolution of V5558 Sgr before and after the maximum is also very similar to that of V723 Cas (Iijima 2007b; Munari et al. 2007; Poggiani 2008, 2010). In the pre-maximum phase the nova shows a featureless F-type spectrum except narrow emission lines $H\alpha$ and $H\beta$ and many weak absorption lines (Iijima 2007a; Naito & Matsuda 2007; Tanaka et al. 2011), which does not resemble to those of classical novae. Fast hot winds (FWHM 1150–1500 km s^{-1}) appeared in the multi-peak episode suggest that mass ejection is associated to the brightening (Munari et al. 2007; Kiss & Sarneczky 2007; Tanaka et al. 2011). During the decline phase, V5558 Sgr had entered the nebular phase and the spectra resemble to those of V723 Cas (Poggiani 2010).

HR Del also showed spectral evolution unlike classical novae (Hutchings 1970; Sanyal 1974; Rafanelli & Rosino 1978). The early spectra before maximum were characterized by relatively narrow emission lines with P Cygni absorption, and the spectral class of F0. Friedjung et al. (1992) examined spectral evolution before maximum and concluded that optically thick winds unlikely occurred before maximum and that the photosphere is almost stationary. HR Del showed several optical maxima which accompany discrete shell ejections (Rafanelli & Rosino 1978; Sanyal 1974). In the nebular phase, spectral evolution was alike to normal novae (Rafanelli & Rosino 1978).

These spectral changes in V723 Cas, V5558 Sgr, and HR Del are consistent with our suggestion that these novae started its outburst from no optically thick wind evolution and, after the multi-peak phase, it changes into an optically thick wind evolution like usual novae.

Table 1 summarizes the outburst properties of these four novae, i.e., the outburst year, duration of maximum phase, presence of multi-peak, information on dust formation, orbital period, estimated WD mass, and suggested type of the companion. For PU Vul, the maximum phase means the phase of flat maximum. For the other three novae, we define the ‘maximum phase’ by the period between the end of quickly rising phase and the last prominent peak. We see that these ‘maximum phases’ last 200–400 days, which is much shorter than the flat maximum phase of PU Vul (8 yr), but much longer than the orbital periods, so there is sufficient time for the companion to orbit many times around the WD before the envelope makes the transition.

PU Vul is a long period binary of $P_{\text{orb}} = 4900$ days and the companion is an M type red giant (RG). During the nova outburst, the WD envelope expands to $\sim 60 R_{\odot}$, which is much smaller than the companion orbit (Kato et al. 2011). Thus, the envelope structure is not affected by the companion. On the other hand, V723 Cas ($P_{\text{orb}} = 0.693$ days = 16.6 hr: Goranskij et al. 2000) and HR Del ($P_{\text{orb}} = 0.214$ days = 5.14 hr: Friedjung et al. 2010; Kürster & Barwig 1988, and references therein) are close binaries and the companion is a dwarf. The orbital period of V5558 Sgr is unknown, but suggested to be as short as normal classical novae, because a large outburst amplitude ($\Delta V > 10$ mag: Naito & Matsuda 2007) suggests that the companion is not an RG. Therefore, in these three novae, the companion should have been deeply embedded in the nova envelope during the outburst.

This is, again, very consistent with that PU Vul (a wide binary) underwent a quiet evolution without strong winds throughout the outburst (Kato et al. 2011). No transition occurred in PU Vul. On the other hand, V723 Cas, HR Del, and V5558 Sgr (close binaries) outburst as a quiet evolution at the beginning, then changed into a wind evolution. The multi-

TABLE 1
TABLE 1. SLOW NOVAE WITH LONG-LASTED PEAK/PRE-MAXIMUM PHASE

Object	Outburst	Maximum Phase	Multi-peak	Dust ^a	P_{orb}	M_{WD}^{b}	Companion
PU Vul ...	1979	8 yr	no	no	4900 days	$\sim 0.6 M_{\odot}$	M giant
V723 Cas ...	1995	400 days	yes	no	16.6 hr	0.58, 0.59 M_{\odot}	dwarf
HR Del ...	1967	320 days	yes	no	5.14 hr	0.595, $\sim 0.9 M_{\odot}$	dwarf
V5558 Sgr ...	2007	200 days	yes	no	unknown	0.58–0.63 M_{\odot}	dwarf ^c

^a PU Vul: there was a debate on the origin of the deep minimum, i.e., to be dust origin or eclipse, but later, it turned clear to be an eclipse. V723 Cas: no dust formed (Lynch et al. 2000). HR Del: no indication of dust in the spectral evolution (Rafanelli & Rosino 1978). V5558 Sgr: no dust formed (Rudy et al. 2011).

^b PU Vul: about $0.6 M_{\odot}$ by Kato et al. (2011) from light curve fitting, V723 Cas: $0.58 \pm 0.07 M_{\odot}$ by Iijima et al. (1998) from absolute B magnitude; $0.59 M_{\odot}$ by Hachisu & Kato (2004) from light curve fitting. HR Del: $0.595 M_{\odot}$ by Kürster & Barwig (1988) from radial velocities; $0.9 M_{\odot}$ by Bruch (1982) from radial velocities. V5558 Sgr: $0.58\text{--}0.63 M_{\odot}$ by Poggiani (2010) from relation between absolute magnitude at maximum and the WD mass.

^c see the text.

ple peaks of these three nova light curves may be a relaxation process associated with the transition. The absence of multiple peaks in PU Vul suggests no transition triggered, which may also support our idea.

No indication of dust formation has been reported for all of the four novae as in Table 1. This is consistent with our suggestion that no/weak optically thick winds occur in these novae, because dust is usually formed in massive winds like OS And and DQ Her.

The estimated WD mass is about $0.6 M_{\odot}$ for all three novae, V723 Cas, HR Del, and V5558 Sgr. Note that some works on slow novae mentioned that this $0.6 M_{\odot}$ is a mass close to the lower limit of WDs having strong nova outbursts as a thermonuclear runaway event (Friedjung et al. 1992; Kato et al. 2002; Tanaka et al. 2011). This argument is based on the calculation by Kovetz & Prialnik (1985) with the old opacity. Recent calculations with the OPAL opacity, however, show that thermonuclear runaway triggers nova outbursts even in much less massive WDs, e.g., in 0.4 and $0.6 M_{\odot}$ WDs (Shara et al. 1993), $0.4 M_{\odot}$ WD (Yaron et al. 2005), and $0.2 - 0.5 M_{\odot}$ WDs (Shen et al. 2009). Therefore, $\sim 0.6 M_{\odot}$ is not the lower mass limit for a WD having nova outbursts. Instead, we emphasize that $\sim 0.6 M_{\odot}$ is a lower boundary for a nova outburst having optically thick winds for solar composition (Kato & Hachisu 2009). Optically thick winds are weak, so it looks like a 'borderline classical nova' (Friedjung & Iijima 2002).

4.3. Composite Light Curves

Figure 6(a) shows theoretical light curves of PU Vul taken from Kato et al. (2011), which consist of only static solutions. The theoretical curve well represents the observational light curve until $t \sim 11$ yr, and then deviates after that when the nova enters the nebular phase. This theoretical curve represents blackbody emission from the WD photosphere and does not include the contribution from nebular emission lines outside the photosphere as well as of the RG companion which dominates in the later phase. Therefore, the theoretical magnitude is much lower than the observation.

We made composite theoretical light curves which mimic the light curves of V723 Cas, HR Del, and V5558 Sgr. Here, we assume that the early phase is approximated by a sequence of static solutions and the later phase by a sequence of optically thick wind solutions. We made two trial light curves; one is the model of $0.55 M_{\odot}$ WD with the chemical composition of $X = 0.55$, $Y = 0.23$, $CNO = 0.2$, and $Z = 0.02$, and the other is an $0.6 M_{\odot}$ WD with the solar composition $X = 0.7$, $Y = 0.28$, and $Z = 0.02$. We switched the solution

from static to wind when the photospheric temperature increases to $\log T_{\text{ph}} (\text{K}) = 3.89$ for the $0.55 M_{\odot}$ WD or to $\log T_{\text{ph}} (\text{K}) = 3.87$ for the $0.6 M_{\odot}$ WD model. The effect of the companion is included in the static phase assuming an $0.4 M_{\odot}$ MS, but not included in the wind phase for simplicity because of their small effects. No rotation effects are included.

Our trial light curves are depicted in Figure 6 (b)-(d). Red lines indicate the model of $0.55 M_{\odot}$ WD and black lines the model of $0.6 M_{\odot}$ WD. We applied the above two trial light curves to the three novae, V723 Cas, HR Del, and V5558 Sgr. The switching epoch from a static to wind evolution is indicated by an arrow. Here, we assumed that the transition occurred ~ 200 days after the outburst. In the very beginning of outbursts, the transition unlikely occurs because the envelope structure may have not yet been close enough to that of a wind solution (see the red line solution in Figure 2). Once the envelope has extended to a giant size, it may take several dynamical timescale for the structure change from static to wind solution. The dynamical timescale is estimated to be $t_{\text{dyn}} \sim (2/GM)^{1/2} r^{3/2} = 21$ days for $r = 6 \times 10^{12}$ cm and $M = 0.95 M_{\odot}$. Note this timescale is roughly consistent with the magnitude variation of these novae which may associate with a relaxation process. Apart from these oscillatory behaviors, our trial light curves are roughly consistent with the observed light curves of these three novae.

Figure 7 shows envelope structures corresponding to each stage of the composite light curve model of the $0.55 M_{\odot}$ WD (depicted by the red lines in Figure 6). The red solid lines in Figure 7 represent the static evolution in the flat maximum, the structure of which hardly changes during the flat maximum, and the black solid lines corresponds to the wind evolution in the decay phase (after the arrow in Figure 6). The green dashed lines indicate the model without the companion effects. We see that, in the presence of a companion, the transition from the static to wind evolution probably occurs, but may not occur without the companion effects because of a large difference between the envelope structures, that is, the green dashed line deviates largely from the rightmost black solid line.

These two trial models adopt a parameter set of the WD mass, companion mass, chemical composition of the envelope, and the orbit, which may be close but not the exact values for each nova. We see, however, our trial light curves reproduce a characteristic properties of observed light curves; the flat phase of static evolution followed by a smooth decline due to wind mass loss. If we choose another set of the parameters, we can also reproduce the flat peak by static solutions and the subsequent decline phase by wind solutions with a dif-

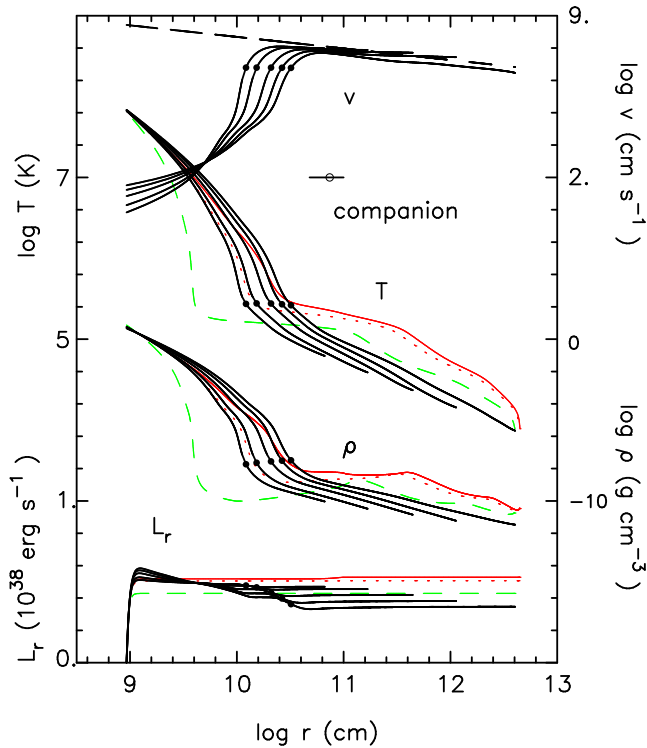


FIG. 7.— Structure change in the evolution model for V723 Cas. The corresponding light curve is shown in Figure 6 by the red lines. The red solid lines represent the static phase of the first 200 days ($\log T_{\text{ph}}(\text{K})=3.892$ and $\log R_{\text{ph}}(\text{cm})=12.65$), during which the structure hardly changes. The black solid lines indicate the structure of optically thick wind phase in which the photospheric temperature increases with time from $\log T_{\text{ph}}(\text{K})=3.87, 4.16, 4.37, 4.59,$ and 4.79 . The corresponding photospheric radius is $\log R_{\text{ph}}(\text{cm})=12.61, 12.05, 11.65, 11.23,$ and 10.82 , respectively. The dotted red lines indicate a rotating static solution of $\eta = 0.2$ and the green dashed lines the static solutions without the companion effects for the same photospheric temperature ($\log T_{\text{ph}}(\text{K})=3.892$) as that of the red solid line. The black dashed line indicates the escape velocity $(2GM_{\text{WD}}/r)^{1/2}$, where $M_{\text{WD}} = 0.55 M_{\odot}$.

ferent decay timescale. The exact parameter fitting is not the aim of the present work, but we expect that we will find a suitable set of the parameters which reproduces the light curve as well as the other observational constraints.

In the present paper, we studied nova outbursts with a 1D approximation. The effects of a companion star are, however, highly aspherical, and the transition may occur in a different way in the different direction. This aspherical nature of the transition may relate to aspherical shapes of nova ejecta, but far beyond the scope of the present analysis.

5. DISCUSSION

5.1. Comparison with Other Works

Common envelope evolution with frictional effects by a companion star has been studied by multi-dimensional hydrodynamic simulations in relation to the formation of close binaries. Taam & Bodenheimer (1989) showed two-dimensional (2D) evolutions of a common envelope, consisting of a $5 M_{\odot}$ RG and an engulfed $1 M_{\odot}$ MS star. Their results demonstrate that frictional process is strong enough to drive a rapid mass outflow from the equatorial plane. Eventually a large part of the envelope (namely $> 3M_{\odot}$) would be ejected and the companion would spiral in. A similar calculation but for a less massive $2 M_{\odot}$ RG and the same $1 M_{\odot}$ MS showed that frictional energy is large enough to eject the envelope, but the companion does not spiral in (Taam & Bodenheimer

1991). Three-dimensional (3D) hydrodynamic simulations by Ricker & Taam (2008) for a binary of a $1.05 M_{\odot}$ RG and an $0.6 M_{\odot}$ MS companion showed that the companion orbit is much reduced by frictional effects of the massive $0.69 M_{\odot}$ RG envelope. In these calculations, the companion efficiently interacts with the massive envelope. This can be understood from Equation (10). As the drag luminosity proportionally increases with the density, we expect very large drag luminosities in massive envelopes.

MacDonald (1980) calculated nova outbursts on a $1.0 M_{\odot}$ WD with a $1.39 \times 10^{-4} M_{\odot}$ envelope and an $0.46 M_{\odot}$ MS companion. The author includes the drag luminosity in 1D approximation, essentially the same as the present work, but the companion's gravity is not included and the opacity is Kramers' law. The author found that the expansion velocity reaches $\sim 300 \text{ km s}^{-1}$, whereas 40 km s^{-1} in the case without drag. The nova duration is not drastically shortened, i.e., the drag luminosity is not effective in mass ejection.

The main difference between ours and MacDonald's (1980) is the opacity. With the OPAL opacity we have obtained the strong optically thick winds of high wind velocity ($\sim 1000 \text{ km s}^{-1}$) for a $1.0 M_{\odot}$ WD and a short nova duration ($\sim 1 \text{ yr}$) as observed. Due to the low density at the orbit, the drag luminosity is very small (Kato & Hachisu 1994). From these reasons, we regard that MacDonald's (1980) results are not inconsistent with ours.

Livio et al. (1990) presented 2D calculations of a common envelope phase of a classical nova on a $1.0 M_{\odot}$ WD with a $0.5 M_{\odot}$ companion and with an initially spherical envelope of mass $5 \times 10^{-6} M_{\odot}$. Their calculation showed rapid mass outflows concentrated in the orbital plane. The mass loss rate reaches $1 \times 10^{-6} M_{\odot} \text{ yr}^{-1}$, corresponding to a timescale of 5 yr for mass ejection, but still being much longer than the observed timescales of novae.

As already pointed out in our previous work (Kato & Hachisu 1991b), Livio et al. (1990) assumed adiabatic gas, in which the drag energy is effectively consumed to push matter upward against the gravity, and results in the strong acceleration of matter. If we adopt non-adiabatic gas, all the drag energy deposition can escape by diffusion process, as already shown in Section 3. Moreover, the authors adopted 60×40 grid points in which frictional energy and angular momentum are deposited into four zones near the companion, which may be insufficient to follow the envelope evolution. Therefore, we suggest that the adiabatic gas and low-resolution grid may be the reason why the authors get strong acceleration of matter concentrated in the equatorial plane while the drag luminosity is very small.

After these works done by MacDonald (1980) and Livio et al. (1990), the OPAL opacity appeared which causes strong acceleration of nova envelopes. We obtained large mass-loss rates and wind velocities as observed (Kato & Hachisu 1994). Once the optically thick winds occur, the drag luminosity has little effects (see Section 3 and also Section 5 of Kato & Hachisu 1994).

To summarize, we may conclude that the drag luminosity is effective in a massive envelope, but in a much less massive envelope, like realistic models of nova outbursts, the drag luminosity is entirely negligible. In other words, the common envelope evolution does not work in nova outbursts even if the companion is deeply embedded in the envelope.

5.2. Spherical (1D) Approximation

We assumed spherical (1D) approximation of the drag energy deposition, in which the energy is deposited in a shell of radius R_{orb} and thickness of $2R_a$. In 2D approximation, the energy is deposited in a torus of diameter of $2R_{\text{orb}}$ with cross section of πR_a^2 . Thus, the energy deposition per solid angle may be

$$\frac{4\pi R_{\text{orb}}^2 \times 2R_a}{2\pi R_{\text{orb}} \times \pi R_a^2} = 2.8 \quad (13)$$

times larger than in our 1D approximation for the case of $0.55 M_{\odot}$ WD and $0.4 M_{\odot}$ MS companion. Here we use the solution of $\log T_{\text{ph}}$ (K) = 3.85 (the model denoted by the black solid lines in Figure 3), in which $R_{\text{orb}} = 7.4 \times 10^{10}$ cm and $R_a = 3.3 \times 10^{10}$ cm. In order to simulate this aspherical effect, we calculated a solution with enhanced drag luminosity by a factor of 2.8. That is, we multiply the right-hand side of Equation (9) by the factor of 2.8. The resultant solution is shown in Figure 3 by dashed lines. The increase of the drag luminosity causes increase of the radiation pressure, which results in the density decrease around the orbit. Therefore, the resultant drag luminosity is 3.1×10^{36} erg s^{-1} , only 1.9 times the original one, 1.7×10^{36} erg s^{-1} . Even if we further increase this factor to 10 as an extreme case, the drag luminosity deposition increases only by 3.4 times of the original one, to 5.7×10^{36} erg s^{-1} . With such enhanced energy deposition, the envelope structure changes, but this effects are relatively small, i.e., less than the change of the companion mass of $0.1 M_{\odot}$ as shown in Figure 3. In actual multidimensional case, the energy deposition due to frictional effects may escape by diffusion process into the pole (rotation-axis) directions, which makes the effects further smaller. Therefore, our 1D approximation may not be far from the multi-dimensional approximations.

We also assumed that the companion mass is distributed in a spherical shell around the orbit. In the extended envelope, the photospheric radius is several tens times larger than the companion orbit as seen in Figure 3. Thus, the 1D approximation may not be so bad in the outer part of the envelope. In the vicinity of the orbit, 2D approximation, this may be close to a time average of a 3D case, gives a stronger gravity which may be roughly estimated as

$$\frac{4\pi R_{\text{orb}}^2 \times 2R_{\text{comp}}}{2\pi R_{\text{orb}} \times \pi R_{\text{comp}}^2} = 3.6, \quad (14)$$

where $R_{\text{comp}} = 2.6 \times 10^{10}$ cm. Therefore, the companion gravity is much effective than our 1D case. The companion masses of V723 Cas, HR Del, and V5558 Sgr are not known, but if it is as low as $\sim 0.1 - 0.2 M_{\odot}$, as in many classical novae, the enhanced gravity may roughly correspond to our massive model of $0.4 M_{\odot}$. Thus, envelope structure may not be largely different from that of our 1D model.

It should be however noted that the center of rotation is the center of mass, which is different from the position of the WD. In this sense, the center of our 1D approximation (i.e., $r = 0$) switches from the WD center in the inner part to the center of mass in the outer part. The intermediate region between them is an interacting region with the companion, which is highly aspherical. Therefore, our 1D model is a rather crude approximation to this intermediate region, which is not easily justified by our 1D model. We need a full 3-D hydrodynamic simulation including radiative diffusion to obtain a definite conclusion to the transition.

5.3. Rotation Law

We also assumed a simple form of angular momentum distribution in the extended envelope. Here we examine how this approximation affects the envelope structure, assuming a different rotation law. Figure 1 shows a trial angular velocity distribution (by the orange solid line) that represents co-rotation with the WD, i.e., $\omega = \Omega$, in the inner part of the companion ($r < R_{\text{orb}} - R_{\text{comp}}$, i.e., $\log r$ (cm) < 10.68), and specific angular momentum conservation in the outside of the binary ($r > 3R_{\text{orb}}$, i.e., $\log r$ (cm) > 11.35). In the intermediate region we connect these two laws in an arbitrary form as shown in the figure. If the nova envelope expands very slowly, it is spun up by the interaction with the companion and gets angular momentum $\sim 1.2 - 1.7R_{\text{orb}}^2\Omega$ per unit mass (see numerical simulations, e.g. Sawada et al. 1984; Jahanara et al. 2005). This may be the maximum value for actual nova outbursts, because expanding speed is not infinitely small (in V723 Cas, the rising timescale is one week). If no further acceleration occurs outside, the angular velocity decreases due to the specific angular momentum conservation. We here assume that the angular velocity decreases according to the specific angular momentum conservation, $l = r^2\omega \equiv 1.7R_{\text{orb}}^2\Omega$ at $r > 3R_{\text{orb}}$.

Figure 1 also shows effective mass fM_r corresponding to the trial angular momentum distribution (the dash-three-dotted line). This effective mass fM_r is constant ($= M_r$) at $\log r$ (cm) < 10.2 as in the other models because the second term of Equation (3) is small, and we have $f = 1$. This means that the angular momentum at the WD surface is so small, that the results are independent of the initial rotation law of the WD envelope. On the other hand, the effective mass fM_r varies corresponding to the change of ω in the middle part and quickly rises as ω decreases in the outer part ($\log r$ (cm) > 11.3).

Figure 4 shows the envelope structure corresponding to the trial rotation law by the orange dash-three-dotted lines. The distributions of the temperature and density in the inner part are very close to those of rapid rotation ($\eta = 0.383$ and 0.45 : red solid and purple dash-dotted lines). As explained previously, a reduced effective gravity due to centrifugal force causes smaller Eddington luminosity in the outer part, and thus, a smaller diffusive luminosity. Therefore, the envelope mass redistributes to balance with a wider local super-Eddington region. As a result, the envelope structure becomes closer to the one without companion, although the structure is very different in the outer part due to irregular variation of fM_r .

From these results, we say that our rotation law defined in Section 2.1 may be too simple but still useful in a qualitative study of possible transition from static to wind evolution of slow novae.

6. SUMMARY

Our main results are summarized as follows.

1. We present an idea of a transition from static evolution to optically thick wind evolution in low-mass WDs ($\sim 0.6 M_{\odot}$). In close binaries, if the effects of a companion are included, the structure of a static envelope becomes close to that of a wind solution. This makes it easy to trigger the transition. In wide binaries, the effects of a companion are not important, and the structure is very different from that of the wind solution. This makes the transition difficult.

2. A transition from static to wind evolution could occur in slow novae such as V723 Cas, HR Del, and V5558 Sgr. The

transition can explain the spectral evolutions of these novae as well as their characteristic light curves. Violent activities like oscillatory behaviors in optical light curves are regarded as some relaxation processes associated with the transition. The presence of a companion deep inside the nova envelopes triggers this transition, which is consistent with the orbital separations in short-period binaries like V723 Cas. On the other hand, no transition occurs in long-period binaries like PU Vul because of no presence of a companion in the nova envelopes.

3. We have calculated the drag luminosity for individual novae/helium novae with various WD masses. The drag lu-

minosity is negligibly small during the outbursts.

We thank the anonymous referee for useful and valuable comments that improved the manuscript. We also thank the American Association of Variable Star Observers (AAVSO) for the photometric data of V723 Cas, HR Del, and V5558 Sgr. This research has been supported in part by the Grant-in-Aid for Scientific Research (20540227, 22540254) of the Japan Society for the Promotion of Science.

REFERENCES

- Barnes, T.B. & Evans, N.R. 1970, *PASP*, 82, 889
 Bondi, H. 1952, *MNRAS*, 112, 195
 Bruch, A. 1982, *PASP*, 94, 916
 Chochol, D. & Pribulla, T. 1997, *Contrib. of the Astron. Obs. Skalnaté Pleso*, 27, 53
 Evans, A., Gehrz, R.D., Geballe, T.R., et al. 2003, *AJ*, 126, 1981
 Fekel, F. C., Joyce, R. R., Hinkle, K. H., & Skrutskie, M. F. 2000, *AJ*, 119, 1375
 Friedjung, M. 1992, *A&A*, 262, 487
 Friedjung, M., Dennefeld, M., & Voloshina, I. 2010, *A&A*, 521, A84
 Friedjung, M., & Iijima, T. 2002, in *AIP Conf. Proc. 637, Classical Nova Explosions*, ed. M. Hernanz & J. Jose' (Melville: NY, AIP), 308
 Goranskij, V. P., Shugarov, S. Y., Katysheva, N.A., et al. 2000, *IBVS*, 4852
 Grygar, J. 1969, *IBVS*, 371
 Hachisu, I., & Kato, M. 2004, *ApJ*, 612, 57
 Hachisu, I., & Kato, M. 2006, *ApJS*, 167, 59
 Hachisu, I., & Kato, M. 2007, *ApJ*, 662, 552
 Hachisu, I., & Kato, M. 2010, *ApJ*, 709, 680
 Hachisu, I., Kato, M., & Cassatella, A. 2008, *ApJ*, 687, 1236
 Hachisu, I., Kato, M., Kato, T., & Matsumoto, K. 2000, *ApJ*, 528, L97
 Hachisu, I., Kato, M., Kiyota, S., et al. 2006, *ApJ*, 651, L141
 Hutchings, J. B. 1970, *Publ. Dom. Astrophys. Obs.*, 13, 347
 Iglesias, C.A., & Rogers, F.J. 1993, *ApJ*, 412, 752
 Iglesias, C. A., & Rogers, F. J. 1996, *ApJ*, 464, 943
 Iijima, T. 2006, *A&A*, 451, 563
 Iijima, T. 2007a, *IAU Circ.*, 934
 Iijima, T. 2007b, *IAU Circ.*, 1006
 Iijima, T., Rosino, L., & della Valle, M. 1998, *A&A*, 338, 1006
 Jahanara, B., Mitsumoto, M., Oka, K., et al. 2005, *A&A*, 441, 589
 Kato, M. 1985, *PASJ*, 37, 19
 Kato, M. 2011, in *Proc. Physics of Accreting Compact Binaries*, The Universal Academy Press, Tokyo (arXiv:1101.2554)
 Kato, M., & Hachisu, I., 1991a, *ApJ*, 373, 620
 Kato, M., & Hachisu, I., 1991b, *ApJ*, 383, 761
 Kato, M., & Hachisu, I., 1994, *ApJ*, 437, 802
 Kato, M., & Hachisu, I. 2009, *ApJ*, 699, 1293
 Kato, M., Hachisu, I., & Cassatella, A. 2009, *ApJ*, 704, 1676
 Kato, M., Hachisu, I., Kiyota, S., & Saio, H. 2008, *ApJ*, 684, 1366
 Kato, T., Uemura, M., Haseda, K., et al. 2002, *PASJ*, 54, 1009
 Kiss, L. & Sarnecky, K. 2007, *IAU Circ.*, 1039
 Kovetz, A. & Prialnik, D. 1985, *ApJ*, 291, 812
 Kürster, M. & Barwig, H. 1988 *A&A*, 199, 201
 Livio, M., Shankar, A., Burkert, A., & Truran, J. W. 1990, *ApJ*, 356, 250
 Lynch, D. K., Rudy, R. J., Mazuk, S. & Venturini, C. 2000, *CBET*, 7492
 MacDonald, J. 1980, *ApJ*, 191, 933
 MacDonald, J., Fujimoto, M. Y., & Truran, J. W. 1985, *ApJ*, 294, 263
 Mannery, E. J. 1970, *PASP*, 82, 626
 Mollerus, B. 1969, *A&A*, 3, 376
 Munari, U., et al. 2007, *IAU Circ.*, 1010
 Naito, H. & Matsuda, K. 2007, *IAU Circ.*, 934
 Nha, I.-S. 1967, *IBVS*, 238
 O'Connell, D.J.K. 1968, *IBVS*, 313
 Onderlička, B., & Vetešník, M. 1968, *Bull. Astron. Inst. Czech.*, 19, 99
 Poggiani, R. 2008, *New Astron.*, 13, 557
 Poggiani, R. 2010, *New Astron.*, 15, 657
 Pohl, E. 1967, *IBVS*, 226
 Prialnik, D., & Kovetz, A. 1995, *ApJ*, 445, 789
 Rafanelli, P., & Rosino, L. 1978, *A&AS*, 31, 337
 Ricker, P. M. & Taam, R. E. 2008, *ApJ*, 672, L41
 Rogers, F.J., & Iglesias, C.A. 1992, *ApJS*, 79, 507
 Rudy, R. J., Russell, R. W. & Sitko, M. 2011, *CBAT*, 9211
 Sanyal, A. 1974, *ApJS*, 28, 115
 Sawada, K., Hachisu, I., & Matsuda, T. 1984, *MNRAS*, 206, 673
 Schaefer, B. E., & Ringwald, F. A. 1995, *ApJ*, 447, 45
 Shankar, A., Livio, M., & Truran, J. W. 1991, *ApJ*, 374, 623
 Shara, M. M., Prialnik, D., & Kovetz, A. 1993, *ApJ*, 406, 220
 Shen, K. J., Idan, I., & Bildsten, L. 2009, *ApJ*, 705, 693
 Stokes, A.J. 1967, *IBVS*, 224
 Taam, R. E. & Bodenheimer, P. 1989, *ApJ*, 337, 849
 Taam, R. E. & Bodenheimer, P. 1991, *ApJ*, 373, 246
 Tanaka, J., Nogami, D., Fujii, M., et al. 2011, *PASJ*, 62, in press
 Yaron, O., Prialnik, D., Shara, M. M. & Kovetz, A. 2005, *ApJ*, 623, 398